Geografiska Annaler: Series A, Physical Geography

ISSN: 0435-3676 (Print) 1468-0459 (Online) Journal homepage: http://www.tandfonline.com/loi/tgaa20

Land cover classification using high-resolution aerial photography in adventdalen, svalbard

Carla Mora, Gonçalo Vieira, Pedro Pina, Maura Lousada & Hanne H. Christiansen

To cite this article: Carla Mora, Gonçalo Vieira, Pedro Pina, Maura Lousada & Hanne H. Christiansen (2015) Land cover classification using high-resolution aerial photography in adventdalen, svalbard, Geografiska Annaler: Series A, Physical Geography, 97:3, 473-488, DOI: 10.1111/geoa.12088

To link to this article: https://doi.org/10.1111/geoa.12088

LAND COVER CLASSIFICATION USING HIGH-RESOLUTION AERIAL PHOTOGRAPHY IN ADVENTDALEN, SVALBARD

CARLA MORA[1], GONÇALO VIEIRA[1], PEDRO PINA[2], MAURA LOUSADA[2] and HANNE H. CHRISTIANSEN[3]

[1]CEG/IGOT, University of Lisbon, Lisbon, Portugal
[2]CERENA-IST, Technical University of Lisbon, Lisbon, Portugal
[3]Geology Department, The University Centre in Svalbard, UNIS, Longyearbyen, Norway

Mora, C., Vieira, G., Pina, P., Lousada, M. and Christiansen, H.H., 2015. Land cover classification using high resolution aerial photography in Adventdalen, Svalbard. *Geografiska Annaler: Series A, Physical Geography*, 97, 473–488. DOI:10.1111/geoa.12088

ABSTRACT. A methodology was tested for high-resolution mapping of vegetation and detailed geoecological patterns in the Arctic Tundra, based on aerial imagery from an unmanned aerial vehicle (visible wavelength – RGB, 6 cm pixel resolution) and from an aircraft (visible and near infrared, 20 cm pixel resolution). The scenes were fused at 10 and 20 cm to evaluate their applicability for vegetation mapping in an alluvial fan in Adventdalen, Svalbard. Ground-truthing was used to create training and accuracy evaluation sets. Supervised classification tests were conducted with different band sets, including the original and derived ones, such as NDVI and principal component analysis bands. The fusion of all original bands at 10 cm resolution provided the best accuracies. The best classifier was systematically the maximum neighbourhood algorithm, with overall accuracies up to 84%. Mapped vegetation patterns reflect geoecological conditioning factors. The main limitation in the classification was differentiating between the classes *graminea*, *moss and Salix*, and *moss, graminea and Salix*, which showed spectral signature mixing. Silty-clay surfaces are probably overestimated in the south part of the study area due to microscale shadowing effects. The results distinguished vegetation zones according to a general gradient of ecological limiting factors and show that VIS+NIR high-resolution imagery are excellent tools for identifying the main vegetation groups within the lowland fan study site of Adventdalen, but do not allow for detailed discrimination between species.

Key words: high-resolution remote sensing, near infrared, UAV, vegetation, Svalbard

Introduction

In recent years a need for mapping Arctic vegetation developed, mainly to better determine climate change impacts on vegetation, and also feedbacks between the biosphere, cryosphere and atmosphere. In the past 100 years warming in the Arctic has been twice the global trend (ACIA 2005; Solomon *et al*. 2007). Svalbard's geographical position and its influence by the North Atlantic drift make it a very sensitive location for recording climate change and its impacts. This has resulted in a growing interest in studies on the High Arctic environment of Svalbard.

Summerhayes and Elton (1923) provide one of the earliest accounts on the ecology of Svalbard. They focused on the description of the vegetation communities and identification of vegetation succession accounting mainly for the stability of the ground. The more recent vegetation classification studies in Svalbard have followed the phytosociological approach, with initial research by Hadač in 1946, later reviewed by Brattbakk in 1981 (Elvebakk 1994). Bratbbakk's vegetation classification was made at a detailed scale 1:10 000, while later, Elvebakk (1994) made a more comprehensive survey of the habitat types in Svalbard. In the National Atlas of Norway of 1986, a vegetation map of Svalbard was presented, but at a small scale for the whole archipelago. Rønning (1996) describes the vegetation of Svalbard and links the vegetation communities with pedoclimatic factors. In 2003 the Circumpolar Arctic Vegetation Map team developed criteria for defining the major bioclimatic zones within the Arctic (Walker *et al*. 2005). Most of the circumpolar units were defined then, but the classification lacked regional aspects (Elvebakk 2005). In order to overcome that, Elvebakk's (2005) map of Svalbard's vegetation already shows more detailed classifications and gradients, benefiting from a comprehensive

DOI:10.1111/geoa.12088

approach. These detailed phytosociological classifications were largely based on classical field surveys.

Remote sensing techniques have also been used for producing vegetation maps at large scales (1:10 000 to 1:50 000) in Svalbard. Nilsen *et al*. (1999a) mapped plant communities using aerial infrared photographs in a small area in Midtre Lövenbreen. On Brøggerhalvøya, the same authors used SPOT imagery for vegetation mapping (Nilsen *et al*. 1999b). Spjelkavik (1995) made a vegetation map for Ny-Ålesund from Landsat TM, and compared the results with existing field-based surveys. A similar approach was presented in the NINA report for several areas in Svalbard (Johansen *et al*. 2009). Zonneveld *et al*. (2004) presented a land use map of Edgeøya using aerial photographs with emphasis on vegetation cover. Most applications in Svalbard have, therefore, used medium resolution imagery, and focused more on the regional variability of the vegetation rather than on identifying local and microscale effects on the vegetation communities and patterns. However, vegetation modelling and monitoring significantly benefit from large-scale maps of sufficient detail and accuracy (Gould *et al*. 2002; Walker *et al*. 2005) and therefore there is interest in using new tools for very-high-resolution mapping, at submetric scales. Recently, Tømmervik *et al*. (2014) used an *unmanned aerial vehicle* (*UAV*) for assessing its application potential for multiscale vegetation index mapping in Svalbard. One of their research areas was Adventdalen, where they showed that the UAV provided reliable measures of NDVI from about 100 m height, especially at the level of vegetation communities. They have also shown that vegetation structure and small shadow effects can induce significant variability in measurements.

At detailed spatial scales, vegetation communities developing during the short Arctic summer are significantly controlled by ground conditions, and a number of microscale patterns form. Vegetation in the Arctic is also highly sensitive to changes in hydrology, snow, dryness and salts (Gould *et al*. 2002) and therefore spatial patterns of vegetation communities can be used for assessing the ecological zonation in sensitive areas, such as those where ice-wedge polygons occur (Walker *et al*. 2005, 2011). Such an approach also contributes to identifying biophysical inter-relationships in the periglacial landscape by using vegetation communities as bioindicators of microscale variations of environmental conditions.

The application of very-high-resolution imagery enables the detection of detailed vegetation patterns, providing special insight into the hydrological, geomorphological, pedological, permafrost and microclimatic conditions, therefore providing an interdisciplinary added value. It complements observations being conducted with other methods, such as field-based geomorphological, geoecological and vegetation mapping. Furthermore, after accuracy evaluation, it can be applied to large and remote areas.

Our main goals were to test the application of very-high-resolution aerial imagery for detailed mapping of lowland tundra vegetation and to identify microscale patterns reflecting geoecological controls in areas of active ice-wedge polygons. Our sub-goals were: (1) to find the best combination of spectral bands and derived data layers providing the best mapping accuracy; (2) to evaluate the performance of different supervised classification algorithms, and (3) to analyze how changes in spatial resolution affect the classification accuracy.

A detailed study area was selected in Adventdalen, where geomorphological and permafrost focused ice-wedge observations are carried out by UNIS (Christiansen 2005). Two types of imagery were used: 20 cm per pixel *RGB* (*visible red, green, blue*) + *NIR* (*near-infrared*) scenes from the *Norwegian Polar Institute* (*NPI*) and 6 cm per pixel UAV-based RGB scenes from Kolibri Geo Services, a private aerial surveying company. The former will be mentioned in the text as NPI and the latter as Kolibri.

Study area

Svalbard is an archipelago located between 74° and 81° N latitude, and 1° and 35° E longitude (Fig. 1). Spitsbergen, where the study area is located, is the largest island in the archipelago. The synoptic air flow over Svalbard is largely affected by the location of the polar front and its seasonal displacements. Generally low-pressure systems near Iceland and high pressures over Greenland, the North Pole and over Russia control Svalbard's meteorology (Hanssen-Bauer *et al*. 1990). This pattern is relatively weak in summer and stronger in winter. Typically from the north, cold anticyclonic, high-pressure air masses extend down to Svalbard, causing longer cold and stable conditions during winter. During stable conditions, cold air accumulates in the bottom of the valleys and air temperature inversions may occur (Humlum *et al*.

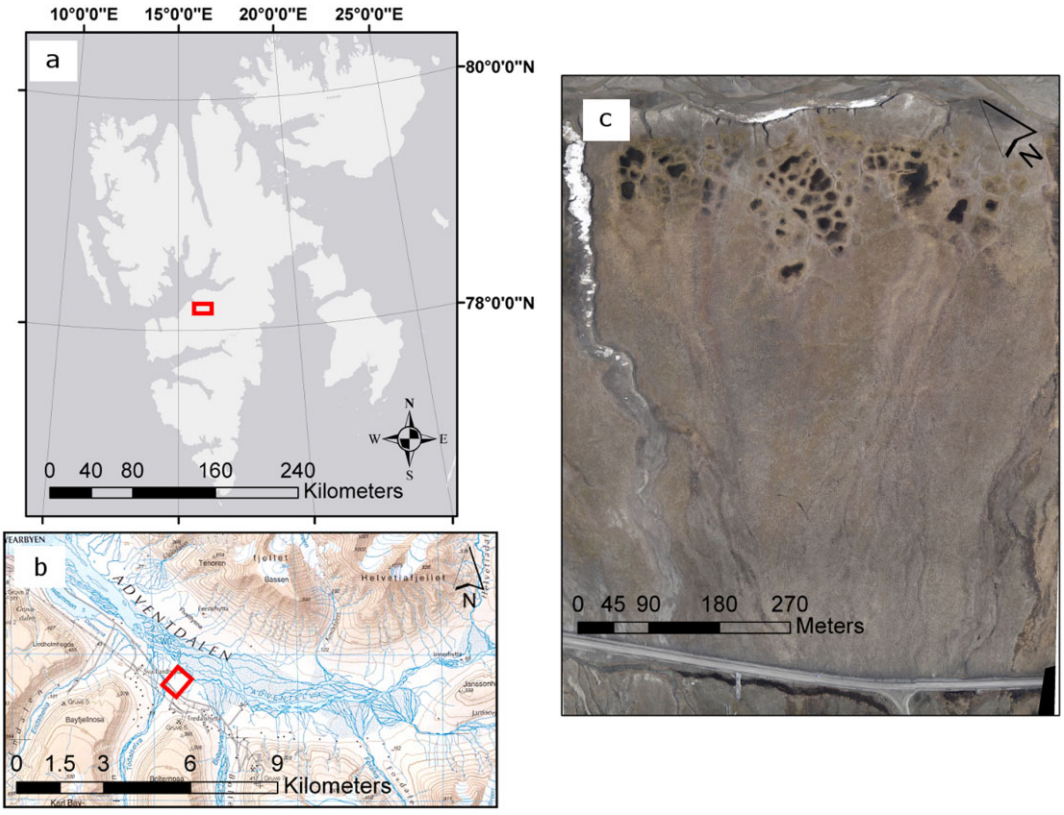

Fig. 1. Location of the study area. (a) Svalbard archipelago (Map created using ArcGIS® software by Esri. ArcGIS® and ArcMap™ is the intellectual property of Esri and is used herein under license. Copyright © Esri. All rights reserved. For more information about Esri® software, please visit www.esri.com.); (b) topographic map: Adventdalen (© Norwegian Polar Institute); (c) study area (S2009 1383_00145 © Norwegian Polar Institute).

2003; Christiansen *et al*. 2013). During the winter season meridional moisture transport along the North Atlantic cyclone track brings moist air masses to Svalbard from the west (Dickson *et al*. 2000). Such events cause large temperature variations, with several above or close to freezing events, heavy snowfall and rain.

In central Spitsbergen the mean annual air temperature is about −5°C at sea level, the mean annual precipitation is around 180 mm and the prevailing winds are westerly or south-westerly (Humlum *et al*. 2005; Christiansen *et al*. 2013). Snowmelt generates most of the runoff in this rather dry environment, and occurs mostly between May and September. The snowmelt from lowland periglacial areas is normally completed during June. Most of Svalbard is in the Northern Arctic Tundra Zone, a transition from the Middle Arctic Tundra Zone in the south and the Arctic Polar Desert Zone in the north (Elvebakk 1999).

The study site is located in the Adventdalen valley in central Spitsbergen, close to Longyearbyen (Fig. 1). The valley is U-shaped and open towards the west. Its flat floor contains the braided river Adventelva, bordered by gently sloping alluvial fans and terraces with complex patterns of ice-wedge polygons (Christiansen 2005). These are mostly low-centred and show orthogonal and polygonal patterns generally with five to six neighbours (Fig. 2). Adventdalen was deglaciated around 10 ka BP and permafrost is estimated to be less than 100 m thick close to the sea (Humlum *et al*. 2003). Most of the periglacial landforms in Adventdalen (e.g. pingos, ice-wedge polygons) formed in the late Holocene and are about 3000 years old (Humlum *et al*. 2003; Christiansen 2005).

The detailed study area is *c*. 0.47 km^2 and includes the long-term ice-wedge polygon monitoring site installed by H.H. Christiansen in 2003 (78° 11′ 09.6″ N, 15° 55′ 26.3″ E), 8 m a.s.l.). The site is

Fig. 2. Aerial view in NE direction of the northern most low-centred ice-wedge polygons of the study area alluvial fan in Adventdalen with their distinct vegetation zonation. The photograph was obtained by Kolibri Geo Services, 19 Aug., 2010, Ulli Neumann, www.geokolibri.com.

located in the distal part of a large alluvial fan from the north-facing valley Todalen, which has been deposited over flat-lying, sedimentary rocks of Early Permian to Eocene age (Dallmann *et al*. 2001; Christiansen 2005). The outer part of the gently sloping fan is covered by 1–2 m of loess (Bryant 1982), that thickens towards the river bank. The fan ends with a cliff 2–3 m high eroded by the river Adventelva into the north part of the fan. Despite the smooth surface of the alluvial fan with very shallow channels vegetated and predominantly buried under the loess cover (Härtel 2011), several geomorphic features indicating active processes occur. In the south, mud-boils are widespread (see Watanabe *et al*. 2012), but northwards, as loess becomes thicker and vegetation more continuous, the mud-boils grade into cracked vegetation polygons (in moss-dominated communities). In the northern part of the fan, low-centred ice-wedge polygonal networks are widespread, which were the subject of recent research (see Christiansen 2005; Härtel 2011). The study sector is therefore located in a stable part of the alluvial fan, with limited erosion, allowing for a continuous vegetation cover to develop.

The ice-wedge polygons are generally 10–20 m in diameter, with troughs from 0 to 35 cm depth and ramparts in the polygon edges that can rise a few decimetres above the polygon centre. The polygonal network consists of first-, second- and third-order ice-wedges, from less than 0.5 m wide to almost 3 m wide. A distinct microscale plant zonation has developed in the ice-wedge polygons, reflecting moisture conditions, snow cover and exposure to wind. Polygonal networks are widespread in the continuous permafrost zone in the lowlands of Svalbard and are typical features of the permafrost environment in the High Arctic (Washburn 1980; Christiansen 2005; Sørbel and Tolgensbakk 2002). The origin of the networks is linked to thermal contraction cracking during cold winter events and seasonal deformation. Spring melt water flows into the open cracks within the permafrost, refreezes and enables the growth of ice-wedges (Washburn 1980). Ice-wedges grow with repeated cycles of cracking, water infilling

and refreezing, and may reach widths of 1–3 m in Svalbard (Humlum *et al*. 2003).

Methods

The distal part of the Todalen alluvial fan is a long-term monitoring area for ice-wedge polygon and mud-boil dynamics (Watanabe *et al*. 2012). Due to easy all-year access, availability of data and knowledge of the area by the authors, it was chosen as a test site for the methodology developed in this paper. The scientific significance of the area and the interdisciplinary nature of research being conducted provide added value to the results presented here.

A field survey was conducted to develop a land cover classification scheme and for collecting ground truth observations used for algorithm training and accuracy assessment. Image classification was tested at different spatial resolutions and with different sets of scenes, including image fusion and derived vegetation indices. Several automatic supervised classifiers have been evaluated and validated against ground truth sets. The best classifier was used to develop a model of land cover and vegetation communities for the study area, identifying spatial patterns resulting from geoecological controls, which would be difficult to depict without this aerial-based approach. The extremely high detail (*c*. 10 cm) limited the use of phytosociological classification schemes. Therefore, we used more generic land cover based vegetation units, which are especially useful for high spatial resolution pattern analysis.

Ground surveying

Field work was conducted in June 2010 and August 2011 to identify the main land cover units, vegetation patterns and to collect ground truth data. The field survey of the vegetation was accompanied by a differential GPS survey of ice-wedge polygon boundaries and topography, allowing for the implementation of a GIS database and for accurate positioning of the field observations. For this purpose, a base station was positioned inside the study area, near to Adventelva and a rover was used for surveying (Trimble R4). One hundred and twenty-one ice-wedge polygons were mapped with DGPS and the distribution of the vegetation species groups was identified in each of the polygons in the field. For better description of the polygons, while in the field a small numbered flag was installed within each of the polygons and only removed at the end of the survey. Our focus was on identifying vegetation according to ecological constraints and especially to use it as a bioindicator of pedoclimatic factors.

The main vegetation units used in the land cover classification were bryophytes, *Salix polaris* and graminoids. They normally occur in mixed formations, and are sensitive to snow, hydrological conditions and wind action. Together with other surface types, such as silty-clay patches, poorly sorted sediment surfaces (generally fluvial silty-sandy-pebbly deposits), snow, water and gravel/non-paved road, they form the nine main surface types that exist in the study area.

The relative location of the surface types were described in the field for each of the 121 ice-wedge polygons that were photographed and mapped with DGPS. Figure 3 shows an example of such a description for polygon 17. The final class grouping was based on the dominant ground cover type, followed by secondary elements in mixed formations.

The ice-wedge polygon boundaries were then plotted over the digital aerial photos using GIS on-screen digitizing. A sample set of land cover units was mapped using the false colour composite. The sample sets were selected for sites where the field description indicated the most homogeneous surfaces and where such surfaces ere also visible in the high-resolution false colour composite. This procedure was supported by inspection of field photographs of individual polygons and allowed for minimizing spectral signature mixing between units. Supplementary points collected with DGPS and with land cover information were sometimes used for helping to define the sample sets. In this way, we were able to maximize the differences in the spectral signatures of each class. The sample sets for non-paved roads, snow and water surfaces were mapped directly in the colour composite, without the need for the field survey, since they show a large contrast and are easy to identify. A total of 70 polygons were defined, with samples ranging between two and nine polygons per class. Those classes which showed more heterogeneous signatures were sampled with more polygons. Depending on the scale of the image, the polygons resulted in a different number of pixels. For the 10 cm pixel size, a total of 47 892 pixels were used in the ground truthing. For running the models we randomly selected 50% of the polygons and the other 50% were used for accuracy checking.

Image classification

Two types of high-resolution digital aerial photographs were used, resampled and fused at 10 and

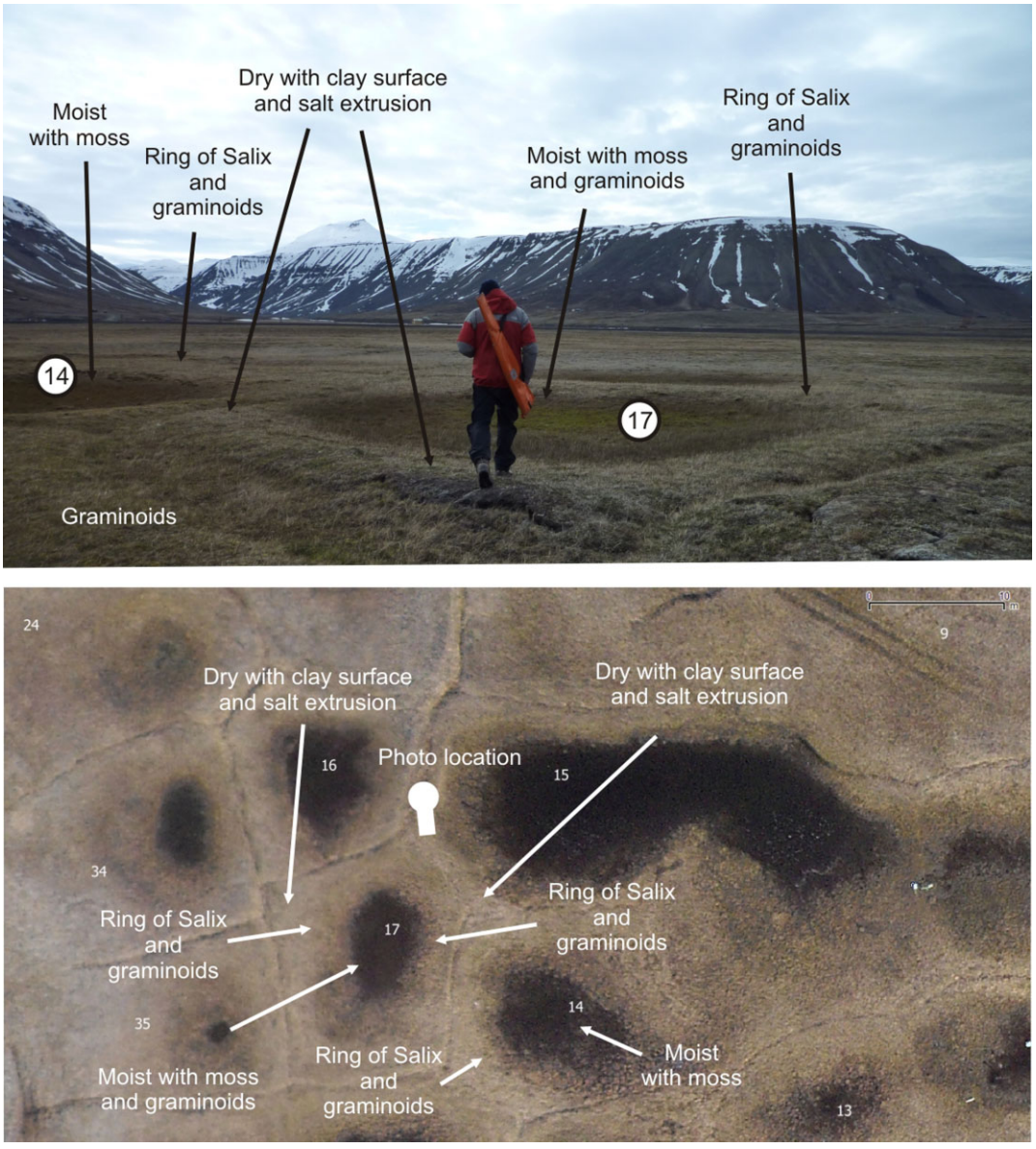

Fig. 3. Example of the field land cover spatial description recorded for each ice-wedge polygon in Adventdalen and example of the same area in the Norsk Polar Institute orthophoto. Case of polygon no. 19.

20 cm resolutions for the vegetation mapping (Fig. 4):

1. high-resolution VIS+NIR orthophotos from 27 Jul., 2009 with *c.* 20 cm spatial resolution (NPI);
2. very-high-resolution VIS photo mosaic from 20 June 2009 with *c.* 6 cm spatial resolution produced by request by Kolibri.

To assess the classification potential of each image, we tested several sets of scenes, with different bands and resolution, by applying four types of supervised classification (parallelepiped, minimum distance, mahalanobis distance and maximum likelihood) in ENVI 4.7. The following band sets were tested:

1. VIS (RGB)+NIR scene from NPI at 20 cm resolution;

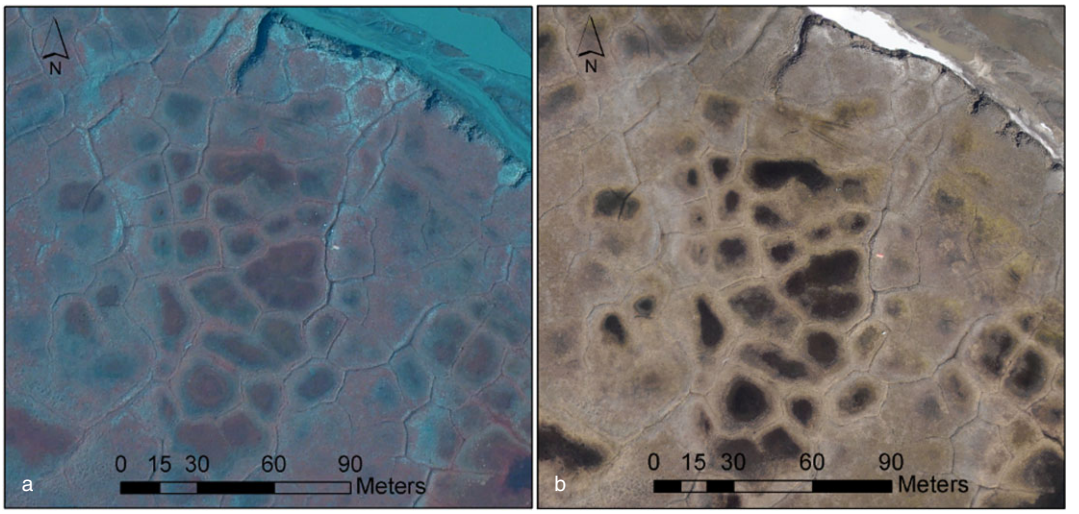

Fig. 4. Samples of the high-resolution aerial photos used for the land cover mapping. (a) Norsk Polar Institute orthophoto (20 cm resolution, false colour composite, S2009 1383_00145 © Norwegian Polar Institute); (b) Kolibri aerial photo (6 cm resolution, colour composite).

2. VIS (RGB) scene from Kolibri at 6 cm resolution;
3. Fused NPI (VIS+NIR) and Kolibri (VIS) at 10 cm resolution;
4. Fused NPI (VIS+NIR) and Kolibri (VIS) at 20 cm resolution;
5. Fused NPI (VIS+NIR+NDVI) and Kolibri (VIS) at 10 cm resolution;
6. Fused NPI (VIS+NIR+NDVI) and Kolibri (VIS) at 20 cm resolution;
7. *Principal components analysis* (*PCA*; four main axes) from the fused NPI (VIS+NIR+NDVI) and Kolibri (VIS) scenes at 10 cm resolution.

The accuracy of each classification scheme was assessed by confusion analysis. For that, the sample set was divided into independent training and validation ground truth sets. The former was used to train the classifier and produce the map, while the latter was used to validate the mapping results. This guaranteed that there was no biasing in the accuracy assessment. The best classification scheme was selected to produce the final vegetation map, and its results and limitations are discussed below.

Our approach is based on the assumption that there were no significant changes in vegetation between the dates of the aerial imagery surveys (June 2009) and our field surveys in June–July 2010 and August 2011. This was verified and confirmed through visual inspection of the terrain. However, seasonal differences in vegetation phenology occur between June and August, resulting in changes in reflectivity due to leaf modifications, especially in *Salix polaris* and *graminea*, but also in changes in moss cover dryness. We hypothesize that the fusion of images from two different dates should provide for better detection of such pattern changes, and even in integrating them in the classification, since the interband variability will be higher than if using scenes from the exact same periods. In this approach we do not use object-based classification, which is a method still not as widely available as the methods we have tested here.

In the image classification stage, after testing with the original field classes, we grouped those vegetation classes which showed mixed spectral signatures, in order to improve the overall accuracy of the classification. This was done iteratively by confusion matrix analysis.

Results and discussion

Land cover classes

The field survey of the alluvial fan study area grouped the main vegetation formations and ground surfaces types into 13 classes, based on the dominant species or on mixed formations, where several types are present. When no vegetation occurred, the ground surface was described according to surface type, e.g. snow, non-paved road,

silty-clay surface, etc. Such an approach focused on identifying vegetation types over patches with a spatial representativeness of over *c.* 1 m^2, which would also be visible in the aerial imagery.

The main vegetation types in the study area were grouped into moss-dominated, *Salix polaris*-dominated and graminea-dominated communities. Variants of these, based on prevailing type, were identified and tested in the image classification process. For the final classification scheme we selected nine classes, of which five are vegetation types. The classification was optimized to obtain a better performance of the classifiers, since there was significant spectral mixing between some mixed classes in initial tests with more classes.

Moss-dominated communities Mosses are typical of moist environments, which can be an indicator of seasonal flooding. Two main divisions were used for the classification (in order to facilitate identification of vegetation classes, we will be using italics when mentioning them): *moss and graminea*, and *moss, graminea and Salix*. The former occurs essentially in the inner part of low-centred polygons, with seasonal ponding and very moist conditions. The latter occurs in moist sites, but well drained, with moss covers occurring together with *Salix polaris* individuals and sparse graminea. It is frequent to see such communities forming a ring around low-centred polygons or in gentle sloping terrain between the flatter and drier *Salix*-dominated plateaus and the lower graminea-dominated sites.

Salix-dominated communities *Salix polaris* is normally associated with graminea, but also appears with mosses. In the areas where it is the dominant vegetation, graminea is also predominant. Such communities occupy the upper edges of polygons under relatively dry and win-exposed conditions. The largest continuous areas occur on the gently sloping surfaces of locally high elevations.

Graminea-dominated communities Graminea are widespread, but as a dominant vegetation it is rarer and occurs essentially in patches of *graminea, moss and Salix*. Such situations occur, either forming a ring in low-centred polygons around a moss-dominated centre, surrounded by *Salix*-dominated formations, or, as larger patches in the lowest and distal part of wide open alluvial fan channels.

Silty-clay surfaces *Silt and clay surfaces* are bare surfaces of loess material that outcrop in convex windswept and dry sites. These surfaces normally show salt extrusions due to intense evaporation and also present sparse individuals of *Salix polaris* and graminea. They are mainly present towards the outer and convex edges of the low-centred polygons, close to the terrace limit, where wind action is stronger, as well as in the western parts of the area, where ground frost activity has generated mud-boil fields. Given our field observations, it is possible that such silty-clay surfaces are over-represented in the map, especially towards the gravel road. This is connected with the problems of classifying the very rough mud-boil terrain, due to significant shadowing effects at the microscale (tens of centimetres) that cause spectral mixing, but may also reflect sediment contamination from the road itself.

Other surface types The other types of surface are non-paved roads and gravel surfaces occurring in the SW part of the site, the water of the Adventelva river, snow banks and vegetation-free sedimentary covers.

Classification method selection

The assessment of the quality of the classification was done by testing different imagery sets and classifiers. The overall accuracies and the kappa coefficients are presented in Table 1. The maximum likelihood classifier provided the best overall accuracy, followed by the mahalanobis distance, some 8–15% below. The parallelepiped and the minimum distance methods showed lower accuracies.

The best band setting was the fused NPI (VIS+NIR) and Kolibri (VIS) at 10 cm resolution using the maximum likelihood classifier, resulting in an overall accuracy of 84% and a kappa coefficient of 0.82. Lowering the spatial resolution to 20 cm resulted in a slight decrease in accuracy to 83.1%. Adding the NDVI band to the classification lowered the accuracy by *c.* 3%, a fact that may be related to increased redundancy and noise in band information. The application of principal component analysis to the image fusion at 10 cm and the selection of the four main factors for the classification, as an attempt to reduce redundancy, resulted in an overall accuracy of 80.4%. Using the original Kolibri VIS scene provided an accuracy of 60.5%, showing the limitations of high-resolution

Table 1. Overall vegetation classification results at the alluvial fan study for different sets of scenes using various supervised classifiers (overall accuracy in percent/kappa coefficient). NPI20: Norwegian Polar Institute at 20 cm resolution (RGB + NIR); Kolibri: Kolibri at 6 cm resolution (RGB); NPI+Kolibri_10, image fusion at 10 cm resolution (all bands); NPI+Kolibri_20: image fusion at 20 cm resolution (all bands); NPI+Kolibri+NDVI_10: image fusion at 10 cm resolution (all bands including NDVI); NPI+Kolibri+NDVI_20: image fusion at 20 cm resolution (all bands including NDVI); PCA NPI+Kolibri_10: image fusion at 10 cm resolution (5 principal components).

	Parallelepiped	Minimum distance	Mahalanobis	Maximum likelihood
NPI20	8.9 / 0.04	65.8 / 0.61	63.6 / 0.58	77.3 / 0.74
Kolibri	27.8 / 0.23	40.6 / 0.34	51.7 / 0.45	60.5 / 0.55
NPI+Kolibri_10	28.7 / 0.24	64.9 / 0.60	71.4 / 0.67	84.0 / 0.55
NPI+Kolibri_20	29.2 / 0.24	67.0 / 0.62	72.5 / 0.68	83.1 / 0.81
NPI+Kolibri+NDVI_10	46.9 / 0.42	64.9 / 0.60	72.0 / 0.68	80.2 / 0.77
NPI+Kolibri+NDVI_20	47.2 / 0.41	67.0 / 0.62	72.3 / 0.68	80.5 / 0.78
PCA NPI+Kolibri_10	51.8 / 0.47	54.6 / 0.60	70.9 / 0.67	80.4 / 0.78

RGB scenes for automatic classification of vegetation. On the other hand, the NPI scene, which includes a NIR band, showed a very high overall accuracy (77.3%).

The analysis of the confusion matrices (Table 2) shows that the sole utilization of the Kolibri image fails mainly in the classification of the vegetation formations, and only classifies accurately those surfaces showing significant spectral differences in the visible spectrum, such as the case of non-paved roads, snow and water surfaces. The NPI scene showed better discrimination of vegetation, but still mixes the class *graminea, moss and Salix*, with *moss, graminea and Salix*. The inclusion of the NDVI also fails in the same classes, and did not show significant improvement. The usage of the principal components fails in the *graminea, moss and Salix*, but also in the *Salix and graminea*, which is mixed with the former.

Classification results using the image fusion at high resolution

Given the results presented above, the best classification method is the one that includes the seven bands resulting from the image fusion at the highest resolution (10 cm). Therefore it was chosen for a detailed discussion and for producing the final vegetation map (Fig. 5).

The overall accuracy obtained was very high, with 84.13% and a kappa coefficient of 0.82. Most classes showed very high producer and user accuracies, with values above 90%, with silty-clay surfaces showing 80.4% in the former and 71.3% in the latter (Table 3). Similarly to the other image sets tested, the main limitation occurred with the graminea-dominated community represented by the class *graminea, moss and Salix*, which showed significant mixing with the moss-dominated community *moss, graminea and Salix*. This resulted in commission errors of 64.6% and omission errors of 74.3%. The producer and user accuracies are as low as 25.7% and 35.4%. This problem may be due to the very low foliar surface of the graminea when compared with mosses and *Salix*, which prevail in the spectral signature. However, this mixing is not very problematic, as it occurs between relatively similar communities, although dominated by mosses. Phenological differences between the field survey of the end of June 2010 and the aerial imagery collected in 2011 may also influence the classification accuracy in the graminea communities. We decided to keep this class since in the vegetation map it forms homogeneous patches of vegetation, which agree with the general patterns of vegetation we observed in the field surveys, with a pattern forming rings around low-centred polygons towards the distal sector of the alluvial fan, in the depressions. Such a pattern reflects an influence of geoecological controlling factors linked to intermediate conditions between those of extreme dryness (in wind-exposed sites), and those of extreme wetness (in ponds or very moist sites). However, further investigation is required to better assess the quality of this component in the vegetation models.

Spatial patterns of land cover classes

The spatial distribution of the land cover classes at the study site in Adventdalen shows relatively homogeneous patches, with patterns reflecting the distribution of geoecological limiting factors such as hydrology, sediment type and topography

Table 2. Confusion matrix with the results of the classification using the maximum likelihood classifier and different sets of bands and images at 10 cm resolution.

	Ground truth								
	Silt-clay surfaces	*Moss, graminea*	*Graminea, moss, Salix*	*Moss, graminea, Salix*	*Gravel/ road*	*Non-sorted sediment*	*Snow*	*Water*	*Salix, graminea*
Kolibri RGB									
Silt-clay surfaces	46	0	1	4	3	31	1	1	1
Moss, graminea	0	89	5	2	0	2	0	1	2
Graminea, moss, Salix	0	3	33	24	0	0	0	0	20
Moss, graminea, Salix	4	2	49	37	0	2	0	2	24
Gravel/road	6	0	0	0	83	32	1	1	0
Non-sorted sediment	36	0	0	0	13	27	0	1	0
Snow	0	0	0	0	0	0	98	0	0
Water	3	1	2	3	0	5	0	89	4
Salix, graminea	4	5	11	29	0	1	0	5	50
NPI RGB+NIR									
Silt-clay surfaces	79	1	2	7	0	3	2	0	1
Moss, graminea	0	93	2	1	0	0	0	0	1
Graminea, moss, Salix	0	1	16	5	0	0	0	0	21
Moss, graminea, Salix	19	4	80	87	0	0	0	0	8
Gravel/road	0	0	0	0	100	2	0	1	0
Non-sorted sediment	0	0	0	0	0	94	29	0	0
Snow	1	0	0	0	0	1	69	0	0
Water	0	0	0	0	0	0	0	99	0
Salix, graminea	0	0	0	0	0	0	0	0	69
NPI RGB+NIR+KOLIIBRI RGB+NDVI									
Silt-clay surfaces	79	0	1	8	0	15	0	0	0
Moss, graminea	0	93	1	1	0	0	0	0	1
Graminea, moss, Salix	0	4	20	8	0	0	0	0	16
Moss, graminea, Salix	18	3	78	81	0	0	0	0	8
Road	0	0	0	0	100	1	0	0	0
Alluvium	1	0	0	0	0	84	8	0	0
Snow	0	0	0	0	0	0	92	0	0
Water	0	0	0	0	0	0	0	99	0
Salix, graminea	2	0	0	2	0	0	0	0	75
NPI RGB+NIR+KOLIIBRI RGB (PCA)									
Silt-clay surfaces	83	0	0	5	0	16	3	0	0
Moss, graminea	0	93	4	3	0	0	0	0	1
Graminea, moss, Salix	0	6	23	4	0	0	0	0	23
Moss, graminea, Salix	15	1	72	88	0	0	0	0	8
Gravel/road	0	0	0	0	100	3	0	0	0
Non-sorted sediment	0	0	0	0	0	81	0	0	0
Snow	0	0	0	0	0	0	97	0	0
Water	0	0	0	0	0	0	0	100	0
Salix, graminea	2	0	0	1	0	0	0	0	68
NPI RGB+NIR+KOLIBRI RGB									
Silt-clay surfaces	80	1	1	4	0	5	0	0	1
Moss, graminea	0	93	1	0	0	0	0	0	1
Graminea, moss, Salix	0	5	26	7	0	0	0	0	16
Moss, graminea, Salix	12	1	72	87	0	0	0	0	7
Gravel/road	0	0	0	0	100	1	0	0	0
Non-sorted sediment	1	0	0	0	0	95	0	0	0
Snow	0	0	0	0	0	0	100	0	0
Water	0	0	0	0	0	0	0	100	0
Salix, graminea	6	0	1	2	0	0	0	0	75

(Fig. 5). The main controls are (1) the very low slope angle of the northeastwards sloping alluvial fan surface; (2) its surficial drainage features; (3) the loess deposits that thicken towards the northeast; and (4) the human impact induced by the road construction and also by its presence. These cause a general grading of the vegetation communities from south to north, passing gradually from *silty-clay*

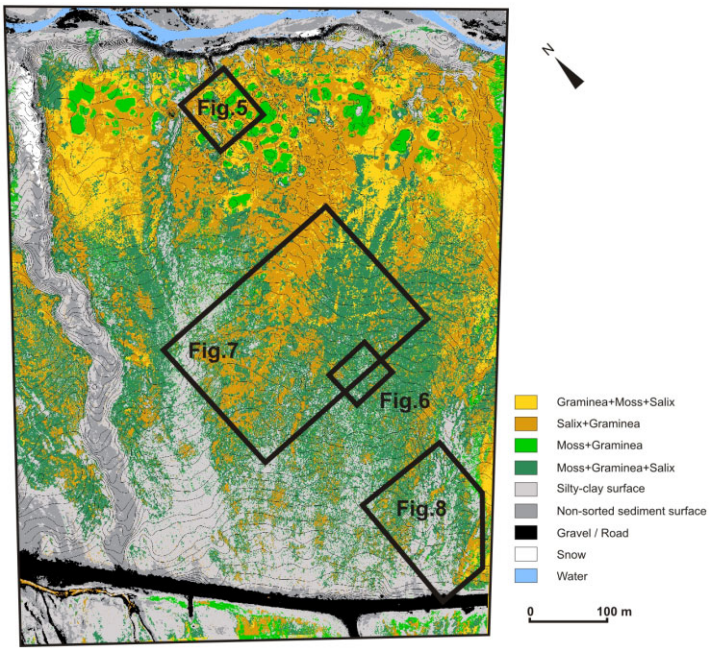

Fig. 5. Land cover of studied alluvial fan area in Adventdalen, modelled using the maximum likelihood classifier and the fusion of the NPI and Kolibri aerial photos at 10 cm pixel resolution. Contour equidistance 25 cm. The polygons indicate the locations of the maps of Figs 5–8.

Table 3. Errors and accuracies of the vegetation classification using a supervised maximum likelihood classifier and the fusion of the NPI and Kolibri aerial photos at 10 cm pixel resolution. Values in percentage.

	Commission errors	Omission errors	Producer accuracies	User accuracies
Silty-clay surfaces	28.75	19.58	80.42	71.25
Graminea+moss+Salix	64.60	74.33	25.67	35.4
Salix+graminea	3.70	24.76	75.24	96.3
Moss+graminea+Salix	48.33	13.44	86.56	51.67
Moss+graminea	3.73	6.82	93.18	96.27
Alluvium	0.82	5.48	94.52	99.18
Road	0.95	0.00	100	99.05
Snow	0.00	0.39	99.61	100
Water	0.00	0.00	100	100

surfaces with scarce vegetation (with frequent mud-boils and other frost features), towards a transitional zone dominated by a mixed *moss+graminea+Salix* and then into the *Salix*-dominated zone. Graminea-dominated patches occur closer to the Adventelva, especially in the lower fan levels.

The general pattern of the vegetation communities is controlled by the presence of a mix of cobbly deposits with a silt-clay matrix that dominates in the south sector, and by the increasing thickness of the loess deposits towards the river bank. Cobbly paleo channels and levees in the fan surface show a concentration of mud-boil activity and clasts in the surface. They give origin to slightly elevated and wind-exposed surfaces that mitigate vegetation development. This is especially frequent closer to the gravel road and gives origin to linear features of silty-clay dominated surfaces.

Salix-dominated communities prevail in the central part of the loess-covered section of the fan, which rise about 75 cm above the fan surface towards the NW and SE. Here graminea-dominated communities are more widespread and the mosaics more complex.

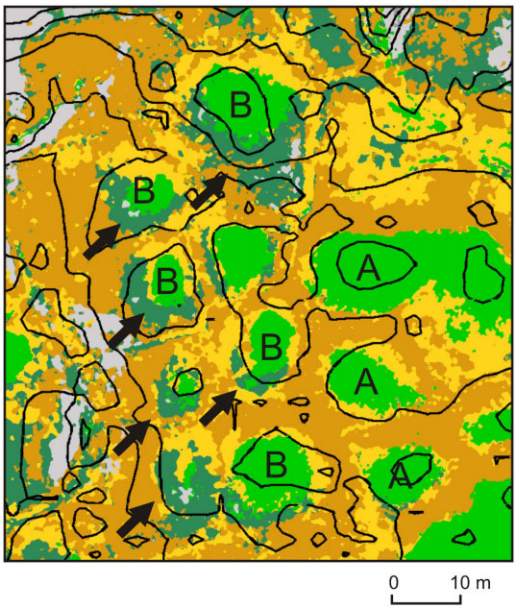

Fig. 6. Vegetation zonation in low-centred ice-wedge polygons as a detail from the map of the land cover of an alluvial fan area in Adventdalen, Svalbard, modelled using aerial photos at 10 cm pixel resolution. (A) Symmetrical zonation; (B) asymmetrical zonation, with arrows indicating *moss+graminea+Salix* communities in the south margin of the depressed centre. See Fig. 5 for colour legend.

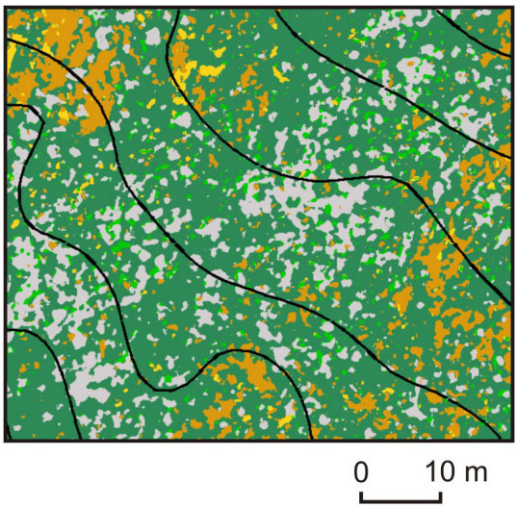

Fig. 7. Vegetation patterns associated with mud-boils as a detail from the map of the land cover of an alluvial fan area in Adventdalen, Svalbard, modelled using aerial photos at 10 cm pixel resolution. See Fig. 5 for colour legend.

The flat-floored channel occurring in the northwest part of the study site, as well as the small channels occurring towards the end of the fan, modify the general vegetation pattern and give origin to bare surfaces of sediment with scarce vegetation growth.

Besides the overall vegetation patterns, the high-resolution map provides insight into the detailed vegetation patterns that are difficult to identify, characterize and quantify in the field, particularly across large areas. One good example is the vegetation patterning in the ice-wedge polygons in the northern part of the fan. The analysis of the upper sector of the terrace shows a clear organization of vegetation around the low-centred polygons (Fig. 6). The lowest part of the polygons shows *moss and graminea* formations, typical of wet conditions. Towards the polygon edges, typically a ring of *graminea and Salix* community occurs, and finally, towards the upper edges, a *Salix*-dominated zone, where conditions are drier. Typical examples of this zonation are indicated in Fig. 6A.

In ice-wedge polygon ramparts, patches of silty-clay surfaces occur, reflecting the dryness and desiccating effect of winds. In the field, salt extrusions are observable in these bare-ground patches. Our remote sensing based mapping also allows for the identification of detailed spatial features in the vegetation, which were not apparent from the field survey. The polygons indicated in Fig. 6B show an asymmetrical zonation of the vegetation communities, with *moss+graminea+Salix* communities prevailing in the south margin of the depressed polygon centres (arrows in figure), and gramineadominated communities in the north margins. This pattern occurs in several polygons and seemingly reflects different geoecological controls at the microscale. The zonation of the polygons is especially well developed in the upper fan surface, where the centres of ice-wedge polygons are lowest. The identification of such a well-developed zonation is an important outcome of this approach.

Other types of features at the microscale also become evident in the vegetation map. Mud-boils are widespread in the south part of the study area. Individual features can be easily identified because of their circular shape, particularly, when the silty-clay centres are surrounded by dense vegetation communities (Fig. 7). However, mud-boils induced problems in our classification, since microtopographical effects induce complex shadowing and result in signature mixing. This may also be the reason for an overestimation of the silty-clay surfaces in the south part of the map.

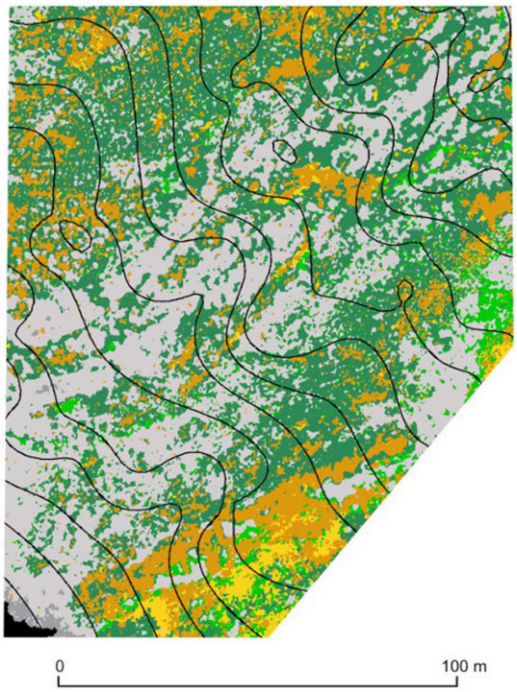

Fig. 8. Elongated silty-clay bare surfaces surrounded by moss communities and related to ice-segregation mounds, as a detail from the map of the land cover of an alluvial fan area in Adventdalen, Svalbard, modelled using aerial photos at 10 cm pixel resolution. See Fig. 5 for colour legend.

In the southeast sector of the study area, silty-clay patches appear elongated, homogeneous and surrounded by moss-dominated communities. Such patterns can be related to the terrain, to elongated mounds that rise a few decimetres above the alluvial fan surface and that seem to be related to increased ice segregation forming palsa-like features (Fig. 8).

Linear features also become evident with our mapping. Figure 9 shows two types of linear vegetation patterns. The white arrows indicate patches dominated by graminea and *Salix* spp. along small fluvial incisions in the alluvial fan. These are natural patterns clearly controlled by topography and moisture availability. On the other hand, black arrows show a narrow linear patch of graminea in the east and of *Salix* spp. in the west, which cross-cuts topography and is a human-made vehicle track. In other sites of the study area, such vehicle tracks are clearly identified in the vegetation map, but in the field they are not so easy to identify. This shows the potential of remote sensing for evaluating human impact in the sensitive tundra surfaces. Even single-pass tracks show clear effects in the landscape, which in the analysed scene corresponded to a disruption of the original moss and graminea-dominated surfaces. The vegetation map also shows vegetation succession along the tracks. In the concave areas, graminea-dominated communities prevail, while in the convex, *Salix*-dominated communities have colonized the tracks.

The image fusion approach using the UAV (RGB) and the NPI aerial photos (RGB+NIR) provided very good classification results and is a significant step forward for the study of high-resolution spatial controls on Arctic tundra vegetation compared with approaches using Landsat imagery (e.g. Johansen *et al*. 2009, 2012). While the latter provide a very good option for regional mapping, the very-high-resolution image fusion method allows for a spatial detail that was not possible to obtain before. The same study area was mapped by Johansen *et al*. (2009, 2012) as showing mainly two main communities: moist tussock tundra, and swamp and wet moss tundra communities. The map that we produced shows the spatial complexity of the mosaics within the communities, as well as the interaction with other units which are not possible to map from the Landsat imagery (e.g. silty-clay surfaces or other sedimentary covers associated with small channels). The new developments presented by Tømmervik *et al*. (2014) with a NDVI camera also support the very high potential of UAV systems, both for mapping at the vegetation community level, but also for monitoring purposes. The fast rate of technological development and price decrease of UAV systems will surely bring very significant advances in very-high-resolution mapping and its applications for vegetation sciences.

Conclusions

The application of very-high-resolution aerial imagery to classify tundra vegetation at the alluvial fan study site in Adventdalen showed very good results, and therefore, the main goal of this work was achieved. The fusion of the NPI VIS+NIR with the Kolibri VIS imagery at 10 cm resolution provided the best accuracies. However, the sole application of the NPI imagery proved to be quite reliable for the classification, which supports its wider application to other parts of the valley floor as this is a standard aerial photography product obtained for larger parts of Svalbard. The best classifier was systematically the maximum neighbourhood

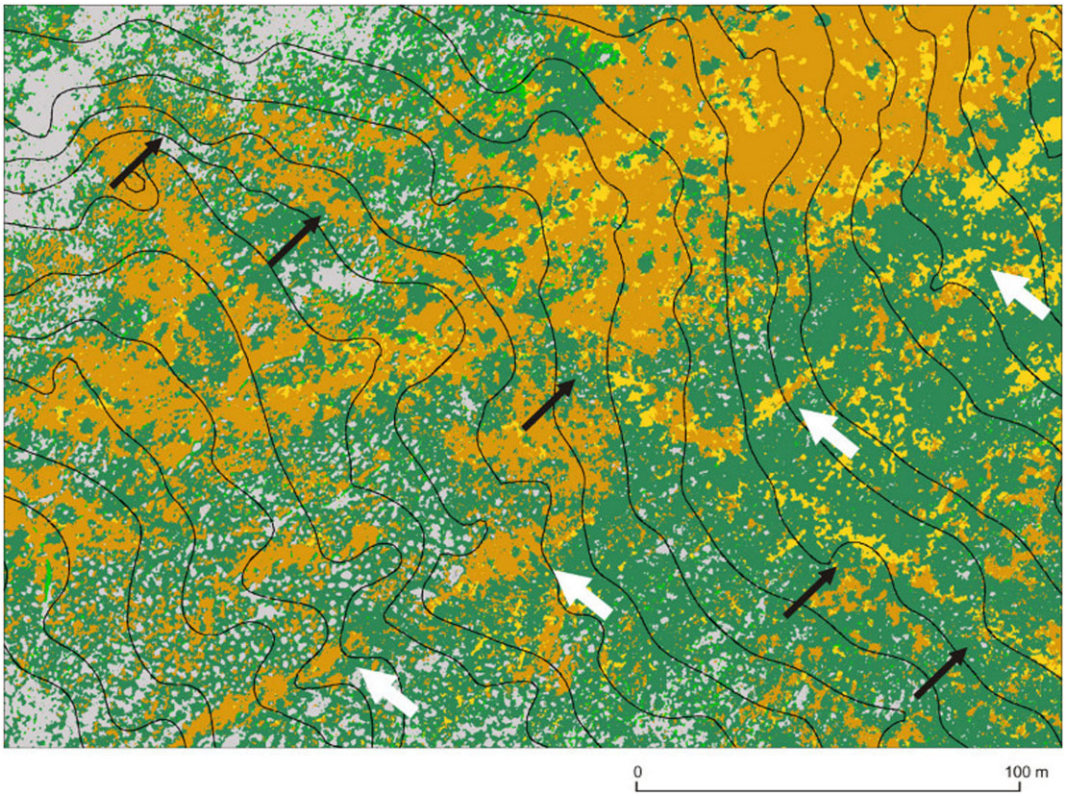

Fig. 9. Natural and anthropogenic linear patches of vegetation in the tundra surface as a detail from the map of the land cover of an alluvial fan area in Adventdalen, Svalbard, modelled using aerial photos at 10 cm pixel resolution. White arrows show natural features along a channel. Black arrows show a vehicle track that cross-cuts topography. See Fig. 5 for colour legend.

algorithm in all tests, resulting in overall accuracies up to 84%. This allowed vegetation patterns to be identified reflecting the geoecological conditioning factors of the area. The main limitation in the classification was in differentiating between the classes *graminea, moss and Salix,* and *moss, graminea and Salix*, which showed significant spectral signature mixing. Silty-clay surfaces were probably overestimated in the south part of the study area due to microscale shadowing effects despite the very low relief.

The results distinguished vegetation zones according to a general gradient of ecological limiting factors: driest conditions, dominated by wind action and salt extrusions, visible in the silt-clay areas, which are also related to the presence of mud-boils and ice-wedge ramparts; transitional zones with *Salix* and graminea; moist areas with mosses; and damp areas with graminea and mosses. This gradient is visible across several scales in the landscape, both along the alluvial fan with a topographical control, but also in a more detailed scale forming a ring structure around low-centred polygons. Microscale effects with a zonation according to aspect on the decimetre scale within polygons were also identified. The identification of such patterns is promising for future studies, since it allows polygons to be characterized based on vegetation structure and therefore characterize their geoecological conditions, which show a clear linkage with sediments, topography, snow and hydrology. Furthermore, the effects of human impact on the tundra vegetation were also emphasized with the sharp identification of linear features related to vehicle tracks visible by the influence on vegetation succession stage.

The results of this detailed comparative analysis show that VIS+NIR high-resolution imagery are excellent tools for the identification of the main vegetation groups within the lowland fan study site of Adventdalen, but they do not allow for a very detailed discrimination between species. The

vegetation associations are complex and only the main groups were identified. A systematic application of this approach to the entire Adventdalen area based on the NPI aerial imagery collection from 2009 will surely provide an excellent exploratory framework for both the geoecology of the fluvioglacial plain and terraces, and also for preliminary assessment of differences between polygon types, which would provide insight into the development of a geomorphological map. An assessment of vehicle track impact and vegetation regeneration is also possible with the application of relatively simple algorithms.

Acknowledgements

This research has been conducted in the framework of project ANAPOLIS (PTDC/CTE-SPA/99041/2008) funded by the Fundação para a Ciência e a Tecnologia. The activities are framed within the Portuguese Polar Program (PROPOLAR). Maura Lousada benefited from a CGD Mobility Grant from the New Generation of Polar Scientists Program and from working in Svalbard as a UNIS masters student. UNIS supported logistics in Svalbard. The UAV imagery was obtained by Kolibri Geo Services. The digital aerial orthophotos were obtained by the Norwegian Polar Institute. We thank the Associate Editor, as well as Dr Hans Tømmervik and two other anonymous reviewers for their numerous comments and suggestions, which contributed to significantly improve the original manuscript.

Carla Mora, Gonçalo Vieira, CEG/IGOT, University of Lisbon, Edifício FLUL, Alameda da Universidade, 1600-214 Lisboa, Portugal.
E-mail: carlamora@campus.ul.pt

Pedro Pina, Maura Lousada, CERENA-IST, University of Lisbon, Instituto Superior Técnico, Av. Rovisco Pais, 1049-001 Lisboa, Portugal

Hanne H. Christiansen, Geology Department, The University Centre in Svalbard, UNIS, P.O. Box 156N-9171 Longyearbyen, Norway

References

ACIA, 2005. *Arctic Climate Impact Assessment*. Cambridge University Press, Cambridge.

Brattbakk, I. 1981. *Bröggerhalvøya, Svalbard*. Vegetasjonskart 1:10,000. K. norske Vidensk. Selsk. Mus Bot. avd. Trondheim, Norsk Polarinstitutt, Oslo 1980.

Bryant, Y.D., 1982. Loess deposits in lower Adventdalen, Spitsbergen. *Polar Research*, 2, 93–103.

Christiansen, H.H., 2005. Thermal regime of ice-wedge cracking in Adventdalen, Svalbard. *Permafrost and Periglacial Processes*, 16, 87–98.

Christiansen, H.H., Humlum, O. and Eckerstorfer, M., 2013. Central Svalbard 2000–2011 meteorological dynamics and periglacial landscape response. *Arctic, Antarctic and Alpine Research*, 4, 6–18.

Dallmann, W.K., Kjærnet T. and Nøttvedt, A., 2001. Geological map of Svalbard 1:100000. Sheet C9G Adventdalen. Explanatory text. *Norsk Polarinstitut Temakart*, 31/32, 1–55.

Dickson, R.R., Osborn, T.J., Hurrell, J.W., Meincke, J., Blindhein, J., Adlandsvik, B., Vinge, T., Alekseev, G., Maslowski, W. and Cattle, H., 2000. The Arctic Ocean response to the North Atlantic Oscillation. *Journal of Climate*, 15, 2671–2696.

Elvebakk, A., 1994. A survey of plant associations and alliances from Svalbard. *Journal of Vegetation Science*, 5, 791–892.

Elvebakk, A., 1999. Bioclimatic delimitation and subdivision of the Arctic. In: Nordal, I. and Razzhivin, V.Y. (eds), *The Species Concept in the High North – A Panarctic Flora Initiative*. The Norwegian Academy of Science and Letters, Oslo. 81–112.

Elvebakk, A., 2005. A vegetation map of Svalbard on the scale 1:3.5 mill. *Phytocoenologia*, 35, 951–967.

Gould, W.A., Edlund, S., Zoltai, S., Raynolds, M., Walker, D.A. and Maier, H., 2002. Canadian Arctic vegetation mapping. *International Journal of Remote Sensing*, 23 (21), 4597–4609.

Hanssen-Bauer, I., Solås, M.K. and Steffensen, E.L., 1990. *The climate of Spitbergen*. DNMI-Report 39/90 KLIMA, 40.

Härtel, S., 2011. *Formation and dynamics of Holocene ice-wedge polygons in Lower Adventdalen, Svalbard*. Diploma Thesis, University of Leipzig and UNIS.

Humlum, O., Elberling, B., Hormes, A., Fjordheim, K., Harald Hansen, O. and Heinemeier, J., 2005. Late-Holocene glacier growth in Svalbard, documented by subglacial relict vegetation and living soil microbes. *The Holocene*, 15 (3), 396–407.

Humlum, O., Instanes, A. and Sollid, J.L., 2003. Permafrost in Svalbard: a review of research history, climate background and engineering challenges. *Polar Research*, 22 (2), 191–215.

Johansen, B.E., Karlsen, S.R. and Tømmervik, H., 2012. Vegetation mapping of Svalbard utilising Landsat TM/ETM+ data. *Polar Record*, 48, 47–63.

Johansen, B., Tommervik, H. and Karlsen, S.R., 2009. *Vegetasjons-Kart over Svalbard basert pa satellittdata. Dokumentasjon av meto-der og vegetasjonsbeskrivelser*. NINA Rapport, 456.

Nilsen, L., Brossard, T. and Joly, D., 1999a. Mapping plant communities in a local Arctic landscape applying a scanned infrared aerial photograph in a geographical information system. *International Journal of Remote Sensing*, 20 (2), 463–480.

Nilsen, L., Brossard, T. and Joly, D., 1999b. Mapping and analysing Arctic vegetation; evaluating a method coupling numerical classification of vegetation data with SPOT satellite data in a probability model. *International Journal of Remote Sensing*, 20, 2947–2977.

Rønning, O.I., 1996. *The flora of Svalbard*. Norwegian Polar Institute, Oslo, Norway, 134.

Solomon, S., Qin, D., Manning, M., Alley, R.B., Berntsen, T., Bindoff, N.I., Chen, Z., Chidthaisong, A., Gregory, J.M., Hegerl, G.C., Heimann, M., Hewitson, B., Hoskins, B.J., Joos, F., Jouzel, J., Kattsov, V., Lohmann, U., Matsuno, T., Molina, M., Nicholls, N., Overpeck, J., Raga, G., Ramaswamy, V., Ren, J., Rusticucci, M., Somerville, R., Stocker, T.F., Whetton, P., Wood, R.A. and Wratt, D., 2007. Technical summary. In: Solomon, S., Qin, D., Manning, M., Chen, Z., Marquis, M., Averyt, K.B., Tignor, M. and Miller, H.L. (eds), *Climate Change 2007: The Physical Science Basis. Contribution of Working Group I to the Fourth Assessment Report of the Intergovernmental Panel on Climate Change*. Cambridge University Press, Cambridge, UK and New York, USA.

Sørbel, L. and Tolgensbakk, J., 2002. Ice-wedge polygons and solifluction in the Adventdalen area, Spitsbergen, Svalbard. *Norwegian Journal of Geography*, 56 (2), 62–66.

Spjelkavik, S., 1995. A satellite-based map compared to a traditional vegetation map of Arctic vegetation in the Ny-Ålesund area. *Polar Record*, 177 (31), 257–269.

Summerhayes, V.S. and Elton, C.S., 1923. Contribution to the ecology of Spitsbergen and Bear Island. *Journal of Ecology*, 11, 214–284.

Tømmervik, H., Karlsen, S.R., Nilsen, L., Johansen, B., Storvold, R., Zmarz, A., Beck, P.S., Johansen, K.S., Høgda, K.A., Goetz, S., Park, T., Zagajewski, B., Myneni, R.B. and Bjerke, J.W., 2014. Use of unmanned aircraft systems (UAS) in a multiscale vegetation index study of Arctic plant communities in Adventdalen on Svalbard. *EARSeL eProceedings*, 13 (S1), 47–52.

Walker, D.A., Patrick, K., Epstein, H.E., Kade, A.N., Vonlanthen, C.M., Raynolds, M.K. and Danie, F.J.A., 2011. Vegetation of zonal patterned-ground ecosystems along the North America Arctic bioclimate gradient. *Applied Vegetation Science*, 14, 440–463.

Walker, D.A., Raynolds, M.K., Daniels, F.J.A., Einarsson, E., Elvebakk, A., Gould, W.A., Katenin, A.E., Kholod, S.S., Markon, C.J., Melnikov, E.S., Moskalenko, N.G., Talbot, S.S., Yurtsev, B.A. and CAVM Team, 2005. The circumpolar arctic vegetation map. *Journal of Vegetation Science*, 16, 267–282.

Washburn, A.L., 1980. *Geocryology: A Survey of Periglacial Processes and Environments*. Halsted Press, John Wiley and Sons, New York.

Watanabe, T., Matsuoka, N. and Christiansen, H.H., 2012. Mudboil and ice-wedge dynamics investigated by electrical resistivity tomography, ground temperatures and surface movements in Svalbard. *Geografiska Annaler: Series A, Physical Geography*, 9, 445–457.

Zonneveld, I.S., Lebouille, M. and Nies, N., 2004. Landscape ecology ('land unit') map of Edgeøya, Spitsbergen with emphasis on vegetation. In: Boschman, N. and Hacquebord, L. (eds), *Permanence in Diversity: Netherlands Ecological Research on Edgeøya*. Spitsbergen, Circumpolar studies, vol. 1. Barkhuis Publishing, Groningen. 103–156.

Manuscript received 28 Jan., 2014, revised and accepted 21 Nov., 2014